the difference between the calculated activation energies for this process and for **9c** → **10c** (29.6 kcal/mol) are much too large to be explained in this way. It therefore seems fairly certain that the conversion of **6** (**9c**) to **7** must be exothermic and that the activation energy for this process must be much less than for **9c** → **10c**. The calculated MERP for the conversion of **9c** (**6**) to **7** via **16** is shown in Figure 9 and the calculated properties of **16**, **7**, and the transition states leading to them are given in Figure 10.

Acknowledgment. We are grateful to Dr. C. Cone for helpful discussions concerning this problem. Our work was supported by the Air Force Office of Scientific Research (Grant AFOSR 75-2749) and the Robert A. Welch Foundation (Grant F-126). The calculations were carried out using the CDC 6400/6600 computer at the University of Texas Computation Center. One of us (D.L.) acknowledges the award of a Robert A. Welch Postdoctoral Fellowship.

References and Notes

(1) Part 1: C. Cone, M. J. S. Dewar, and D. Landman, *J. Am. Chem. Soc.*, **99**, 372 (1977).
(2) F. W. McLafferty and J. Winkler, *J. Am. Chem. Soc.*, **96**, 5182 (1974).
(3) (a) For a general reference, see J. T. Bursey, M. M. Bursey, and D. G. I. Kingston, *Chem. Rev.*, **73**, 191 (1973), and references cited therein; (b) J. M. S. Tait, T. W. Shannon, and A. G. Harrison, *J. Am. Chem. Soc.*, **84**, 4 (1962); (c) P. Brown, *ibid.*, **90**, 2694, 4459 (1968); (d) *Org. Mass Spectrom.*, **2**, 1085 (1969); (e) R. H. Shapiro and J. W. Serum, *ibid.*, **2**, 533 (1969).
(4) M. J. S. Dewar, *J. Am. Chem. Soc.*, **74**, 3355 (1952); "The Molecular Orbital Theory of Organic Chemistry", McGraw-Hill, New York, N.Y., 1969.
(5) M. J. S. Dewar and R. C. Dougherty, "The PMO Theory of Organic Chemistry", Plenum Publishing Corp., New York, N.Y., 1975.
(6) (a) R. Westwood, D. H. Williams, and A. N. H. Yeo, *Org. Mass Spectrom.*, **3**, 1485 (1970). (b) This is an example of the general process suggested by Beynon et al. in the molecular ion of nitrobenzene: J. H. Beynon, R. A. Saunders, and A. E. Williams, *Ind. Chim. Belge.* **No. 4**, 311 (1964).
(7) J. L. Franklin, J. G. Dillard, H. M. Rosenstock, J. T. Herron, K. Draxl, and F. H. Field, *Natl. Stand. Ref. Data Ser., Natl. Bur. Stand.*, **No. 26**, 1 (1969).
(8) We established that this was again the easiest path from **9** to **10**.
(9) M. J. S. Dewar and N. Trinajstić, *Croat. Chem. Acta*, **42**, 1 (1970).
(10) (a) E. Heilbronner and K. Hedberg, *J. Am. Chem. Soc.*, **73**, 1386 (1951); (b) M. Kimura and M. Kubo, *Bull. Chem. Soc. Jpn.*, **26**, 250 (1953); (c) M. Kubo and K. Kimura, *ibid.*, **27**, 455 (1954); (d) K. Kimura, S. Suzuki, M. Kimura, and M. Kubo, *J. Chem. Phys.*, **27**, 320 (1957). (e) K. Kimura, S. Suzuki, M. Kimura, and M. Kubo, *Bull. Chem. Soc. Jpn.*, **31**, 1051 (1958).
(11) Tait et al.[3b] have claimed that *p*-hydroxytoluene rearranges to give **10b** in the mass spectrometer, whereas *p*-methoxytoluene gives the *p*-methoxybenzyl cation (**3**). Their evidence, however, was derived entirely from a Hammett-type plot of appearance potentials of $C_7H_6X^+$ ions vs. σ^+ values. Now σ^+ values refer to reactions in solution; here hydrogen bonding to the solvent should greatly increase the σ^+ value of hydroxyl relative to methoxyl. In the gas phase, the effective σ^+ value for hydroxyl should be significantly less than that for methoxyl because the −I effect of methyl in the latter will increase its electron donating power. It therefore seems likely that the deviation of the point for *p*-hydroxytoluene from the line in the plot of Tait et al.[3b] in fact reflected the use of an inappropriate value for σ^+.
(12) (a) M. M. Bursey, *Org. Mass Spectrom.*, **2**, 907 (1969); (b) J. H. Beynon, M. Bertrand, and R. G. Cooks, *J. Am. Chem. Soc.*, **95**, 1739 (1973).
(13) O. Chapman, D. Heckert, W. Reasoner, and S. Thackaberry, *J. Am. Chem. Soc.*, **88**, 5550 (1966), and references cited therein.
(14) R. C. Bingham, M. J. S. Dewar, and D. H. Lo, *J. Am. Chem. Soc.*, **97**, 1294, 1302 (1975).

Semiempirical Calculations of Model Oxyheme: Variation of Calculated Electromagnetic Properties with Electronic Configuration and Oxygen Geometry

Robert F. Kirchner and Gilda H. Loew*

Contribution from the Department of Genetics, Stanford University Medical Center, Stanford, California 94305. *Received August 26, 1976*

Abstract: The iterative extended Hückel method is used to characterize the electronic structure of model oxyferroporphyrin complexes with *N*-methylimidazole as an axial ligand. Twenty-two conformations of the dioxygen ligand are considered. A bent, end-on dioxygen ligand geometry with low energy off-axis displacements and a low energy barrier to rotation about the Fe-O axis possibly coupled to a large amplitude bending mode of the Fe-O-O bond is favored. The electric field gradient at the iron nucleus observed as quadrupole splitting in Mössbauer resonance is calculated for each dioxygen ligand geometry in six likely electronic ground-state configurations. A paired iron(II)-dioxygen configuration yields the large negative electric field gradient observed for oxyhemoglobin and synthesized model compounds. The observed temperature dependence may be accounted for by rotation about the Fe-O axis. Net atomic charges, overlap densities, and variation in iron-ligand interactions as a function of dioxygen ligand geometry as calculated by the iterative extended Hückel method are reported.

Properties attributed to the iron active site of heme proteins have been measured for both oxyhemoglobin and recently synthesized[1] model compounds that show reversible oxygenation. Mössbauer resonance of the proteins[2] and of the model compounds[3] has been used to probe the electron distribution around the iron nucleus. Magnetic susceptibility,[4] electronic transitions,[5] and infrared stretching frequencies[6,7] have been measured in order to further elucidate the binding of dioxygen to iron porphyrins. An x-ray diffraction study of the oxygenated model compound has been performed[3] to determine the structure of the iron-dioxygen unit. Yet, despite the large amount of experimental data, two major areas of interest in the complete understanding of oxyhemoglobin remain largely unresolved: (1) differentiation between a formal iron(II)-dioxygen or iron(III)-superoxide electronic configuration to best describe the interaction of molecular oxygen with the iron porphyrin unit, and (2) determination of the geometry of the dioxygen ligand in the heme pocket, allowing for the possibility of a number of low energy conformations.

Similarities between the electronic spectra of oxyhemoglobin and alkaline met hemoglobin led to the suggestion[8-10] of a formal iron(III)-superoxide electronic ground-state configuration for oxyhemoglobin. However, the similarities are associated primarily with porphyrin $\pi \rightarrow \pi^*$ transitions.[11] Therefore, no direct conclusions can be made regarding the electronic structure of iron and oxygen.[12] More recently three broad transitions in the regions 10 000, 20 000, and 30 000 cm^{-1} were observed in the single crystal polarized absorption

spectra of oxyhemoglobin[5] and oxymyoglobin.[13] Although these transitions are believed to involve charge transfer to oxygen, definitive assignments have not been made.

The proposal that oxyhemoglobin is best described by an iron(III)-superoxide configuration was evoked[2] primarily to account for the large quadrupole splittings observed in Mössbauer resonance of the protein and of the model compounds. If covalency effects are neglected, such splittings are considered anomalous for a low-spin iron(II) configuration. However, extensive delocalization by forward and back donation from and to the ligands can cause considerable asymmetry in the electric field around the iron and result in a net charge transfer from iron to dioxygen even with an iron(II)-dioxygen configuration. This totally paired configuration can also account for the observed diamagnetism of oxyhemoglobin.[4] With a biradical iron(III)-superoxide configuration, the diamagnetism can only be rationalized by assuming "antiferromagnetic" coupling of the two unpaired electrons.

To predict the electronic configuration and geometry of the $Fe-O_2$ bond, Caughey and colleagues[6] have measured the infrared stretching frequency of dioxygen in oxyhemoglobin. Comparing the measured value (1107 cm^{-1}) with metal-dioxygen complexes known to have a doubly coordinated (Griffith) structure with equivalent oxygen atoms (~850 cm^{-1}) or an end-on, singly coordinated (Pauling) structure with inequivalent oxygen atoms (~1125 cm^{-1}), they concluded that the $Fe-O_2$ complex had a bent, end-on conformation with an iron(II)-dioxygen electronic configuration. Excess amounts of anionic ligands such as Cl^-, CN^-, and N_3^- were observed to displace dioxygen. However, due to the slow rate of displacement only a small amount of superoxide anionic character was ascribed to the charge of the oxygen molecule, perhaps induced as a result of protonation and incipient reaction with the nucleophile.[7]

An x-ray structure analysis of a model of the oxyheme unit[3] showed the oxygen ligand bound to the iron in a bent, end-on (Pauling) fashion.[14] Two nearly symmetry equivalent geometries corresponding to a 90° rotation about the iron-oxygen bond seemed to be favored. However, the crystallographic data indicated a large disorder and consequent ambiguity in the position of the second oxygen atom. Due to the uncertainties, the possibility of a triangular (Griffith) structure[15] with both oxygen atoms coordinated to iron has not been entirely eliminated.

Thus, in spite of a large number of experimental investigations, the electronic structure and geometry of the oxyheme unit remain in doubt. Some theoretical calculations have been made to try to resolve these uncertainties and to account for the observed properties of oxyhemoglobin.

Symmetry restricted iterative extended Hückel calculations were performed by Zerner et al.[16] on a model of oxyheme. The results of these calculations were used to tentatively identify the transitions observed in the single crystal polarized absorption spectra and later used by Weissbluth et al.[17] to predict a positive value for the low-temperature quadrupole splitting of oxyhemoglobin. The model of oxyheme consisted of a regularized porphin ring with the iron 0.42 Å out of the heme plane, a water molecule for one axial ligand, and dioxygen either doubly coordinated to iron (with the O-O axis parallel to an N-Fe-N axis) or singly coordinated to iron (with the O-O axis perpendicular to the heme plane). In a more recent iterative extended Hückel calculation, Aronowitz et al.[18] conclude that an off-axis, slightly tilted oxygen geometry can best account for the observed absorption spectra based primarily upon assignment of the lowest energy transition to $a_1[a_{2u}(\pi)] \rightarrow b_1[O_2(\pi^*)]$. However, while this transition has been identified as involving oxygen,[5] it has not been definitively assigned from the many possibilities obtainable from calculated orbital promotion energies together with the estimated exchange corrections of Zerner et al.[5,16] At present it appears that several different geometries of the $Fe-O_2$ bond with a formal iron(II)-dioxygen ground state can fit the spectra equally well.[12]

Extended Hückel calculations were performed by Halton[19,20] for a very small model of oxyheme which included only iron, oxygen, and nitrogen atoms with select valence orbitals on each. A negative field gradient could be obtained with this model only by addition of two extra electrons in the system.

Heitler-London calculations reported by Seno et al.[21,22] for a model oxyheme system predict a singlet ground state consisting primarily of an electron configuration with four unpaired electrons (two on the iron and two on the oxygen). A similar ground state was reported by Goddard et al.[23] for ab initio generalized valence bond configuration interaction calculations (GVB-CI) on an isolated iron-dioxygen unit. A parallelism between dioxygen binding to iron and that found for ozone was assumed with a Fe-O-O bond angle of 90° and a forced ground-state configuration of $(d_{xy})^2(d_{yz})^2(d_{xz})^1(d_{z^2})^1(d_{x^2-y^2})^0$ on the iron. The calculations yielded a negative field gradient at the iron nucleus and also preserved the strong electronic transition of ozone at 40 000 cm^{-1}, which was assumed to correspond to a $\pi_O \rightarrow \pi_O^*$ transition of dioxygen in the oxyheme complex. However, a high-frequency internal oxygen transition can be accounted for on the basis of several structural models, since both molecular oxygen and superoxide anion also exhibit bands in the 40 000-cm^{-1} region.[12,24,25] Moreover, the calculated value of the quadrupole splitting is suspect due to limitations in the procedure. The estimate of the electric field gradient did not include delocalization of the iron orbitals (covalency effects) from the assumed atomic orbital population. Forcing the $d_{x^2-y^2}$ orbital to stay totally unoccupied neglects a large positive contribution to the field gradient, while arbitrarily placing an electron in the d_{z^2} orbital adds a negative one. In addition, cross terms in the d-orbital contribution were not calculated. In order to obtain coordinate independent principal axis values used in calculating quadrupole splittings, the full nine-component field gradient tensor must be diagonalized.

Recently a LCAO-MO-SCF ab initio calculation has been performed by Dedieu et al.[26,27] on an oxyferroporphyrin model compound both with the dioxygen ligand singly coordinated to the iron in a bent fashion or doubly coordinated to the iron, the latter resulting in a higher energy. An estimation of the barrier to rotation about the iron-oxygen axis was made. In an attempt to identify the ground-state electronic configuration, the total energies of several spin paired and spin unpaired biradical iron(III)-superoxide configurations were compared to that calculated for a totally paired iron(II)-dioxygen configuration. Ammonia was used to approximate the proximal and in some cases the distal histidine residues. One calculation was performed with imidazole as a sixth ligand. However, no properties other than net atomic charges from a Mulliken population analysis were calculated.

We have previously reported[28] preliminary results of iterative extended Hückel calculations for a number of oxyferroporphyrins with dioxygen singly coordinated to iron and *N*-methylimidazole as the second axial ligand. The large negative field gradient observed for oxyhemoglobin and synthesized model compounds could be explained by a totally spin paired diamagnetic iron(II)-dioxygen ground state, while the charge distribution showed superoxide anionic character on the oxygen.

In the work reported here we have included more variations of the oxygen geometry, rotation of the imidazole ligand, and a variety of possible charge transfer configurations with two half-filled orbitals. Finally, we have extended our field gradient calculation to completely include all of the off-diagonal terms

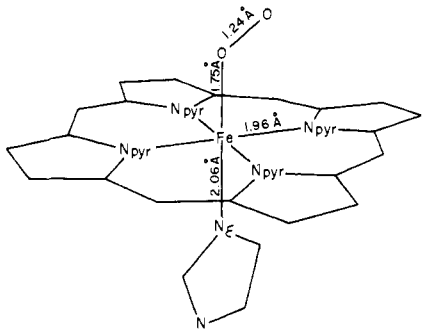

Figure 1. Model of oxyheme taken from x-ray structure analysis of synthesized oxygenated model compounds.

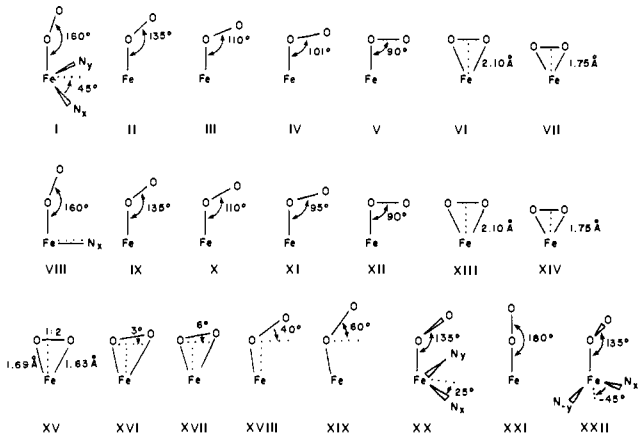

Figure 2. Twenty-two structures obtained by variation of the dioxygen ligand geometry. In conformers I through VII the projection of the dioxygen ligand onto the heme plane bisects the pyrrole nitrogens N_x and N_y ($\tau = 45°$). In conformers VIII through XIX the projection of the dioxygen ligand onto the heme plane lies on a pyrrole nitrogen axis N_x ($\tau = 0°$). In conformer XX $\tau = 25°$. In conformer XXII $\tau = -45°$.

in the atomic orbital basis. Due to the mixing of atomic orbitals in the calculated molecular orbitals of the low symmetry oxyheme compounds at certain oxygen geometries, these terms were found to have a major effect and modify some of the results reported earlier. A more complete account of the work is given here.

Method

Eigenvalues and eigenvectors were calculated using the semiempirical all valence iterative extended Hückel procedure parameterized[16] for iron-porphyrin compounds.

The basic model used for the oxyferroheme complex is a simplified version of the recently synthesized[1] model oxyheme complex. As shown in Figure 1, the model consists of a nearly planar porphine ring and two axial ligands, *N*-methylimidazole and molecular oxygen. The geometry of the porphine ring and the imidazole ligand was taken directly from the x-ray analysis of the model compound.[29] Twenty-two variations of the oxygen ligand geometry were considered as shown in Figure 2. These include the two conformers found in the x-ray analysis (structures II and XXII), variations of the Fe-O-O bond angle (θ) from 180 to 90° (structures XXI and I through V), rotations about the Fe-O bond (dihedral angle $\tau_{N_{pyr}\text{-Fe-O-O}}$ is the angle between the two planes defined by the atoms N_{pyr},Fe,O and Fe,O,O) from $\tau = 45°$ to $\tau = 25°$ (structure XX) and $\tau = 0°$ (structures VIII through XII), doubly coordinated symmetric conformations (structures VI, VII, XIII, and XIV), and a number of asymmetric "tilted" structures which combine features of the singly coordinated and doubly coordinated dioxygen geometries (structures XV through XIX). For the oxygen conformation reported in the crystal structure (II), four additional imidazole geometries corresponding to rotation around the Fe-N_ϵ bond were considered.

Table I. Electronic Configurations Used in Calculation of Quadrupole Splitting

Configuration	Orbital occupation					
	$[d_{\pi-} + \pi_{O-}]$	$[\pi_{O+} + d_{\pi+}]$	$[b_{2g}\text{-}(d_{xy})]$	$[a_{2u}\text{-}(\pi_N)]$	$[d_{\pi+} - \pi_{O+}]$	$[\pi_{O-} - d_{\pi-}]$
A	2	2	2	2	2	0
B	2	2	2	2	1	1
C	2	2	2	1	2	1
D	2	2	1	2	2	1
E	2	1	2	2	2	1
F	1	2	2	2	2	1

The eigenvectors obtained from the molecular orbital calculations of each dioxygen and imidazole geometry were used to calculate quadrupole splittings for a number of electronic configurations shown in Table I. When no assumptions were made regarding spin or oxidation state of the iron and dioxygen ligand, the iterative extended Hückel procedure yielded a low-spin iron(II) coupled to a singlet oxygen molecule (configuration A). Five biradical configurations were formed by vertical promotion of an electron from the orbitals of the spin paired Fe(II)-O_2 description. Local contributions of the nine components of the field gradient at the iron nucleus were evaluated, principal axis values and anisotropy obtained, and quadrupole splittings calculated with a shielding factor value of $(1 - R) = 0.68$, average values of $\langle r^{-3}\rangle_{3d} = 5.00$ au and $\langle r^{-3}\rangle_{4p} = 2.04$ au, and a value of the iron nuclear quadrupole moment $Q = 0.187$ b. Details of the formulation of the calculation are presented elsewhere.[30]

Results

A regularized iron-porphine complex has D_{4h} symmetry. Depending upon the dioxygen geometry, the symmetry of an axially liganded model would be reduced to C_2 or C_s. If the second axial ligand *N*-methylimidazole is also considered, any remaining symmetry is lifted. Further, since the iron-porphine core has not been regularized, all of the models for oxyheme have C_s symmetry. It is customary though to identify the molecular orbitals, whenever possible, according to the representations of D_{4h} symmetry.

Eigenvalues, predominant atomic orbital coefficients, and percent iron and oxygen character in the highest occupied and lowest empty molecular orbitals are given in Table II for the end-on crystal structure (II) and in Table III for a doubly coordinated structure (VI). In both geometries, the predominantly $d_{x^2-y^2}$ and d_{z^2} antibonding molecular orbitals are empty, but have low-energy bonding partners, while the d_{xy} orbital is fairly localized and occupied. On the other hand, the interaction of the d_{xz} and d_{yz} orbitals with the two originally degenerate, singly occupied π orbitals of molecular oxygen is quite different in the two types of dioxygen ligand geometries. As shown in Table IV, there are two symmetry combinations of the d_{xz} and d_{yz} orbitals and two combinations of the oxygen π orbitals which interact. Depending on the iron-dioxygen geometry, these orbitals combine in different ways to form four delocalized iron-oxygen orbitals as shown in Figure 3.

In the bent, end-on dioxygen ligand geometry, there is extensive interaction of $d_{\pi+}$ with π_{O+} and $d_{\pi-}$ with π_{O-}. The higher energy partner of the $d_{\pi-} \pm \pi_{O-}$ pair has predominantly π_{O-} character and is unoccupied (MO 83), while the lower energy occupied partner shows more mixing (MO 77). The two occupied $d_{\pi+} \pm \pi_{O+}$ orbitals are intermediate in energy with the higher energy partner having predominantly $d_{\pi+}$ character

Table II. Eigenvalues and Eigenvectors Calculated for Model Oxyheme[a]

Energy[b]	Symmetry[c]	$(MO)^{occ}$	Principal atomic orbital coefficients[d]	%Fe[e]	%O[e]
−7.79	$a_1[b_{1g}(d_{x^2-y^2})]$	$(87)^0$	$0.74d_{x^2-y^2} + 0.29d_{z^2} \pm 0.29N_{\pm x}p_x \mp 0.43N_{\pm y}p_y$	49	1
−7.92	$a_1[a_{1g}(d_{z^2})]$	$(86)^0$	$0.79d_{z^2} - 0.27d_{x^2-y^2} \mp 0.34N_{\pm x}p_x + 0.33O'p_z - 0.43N_\epsilon p_z$	55	10
−9.01	$b_1 + b_2[e_g(\pi^*)]$	$(85)^0$	$\pm 0.35N_{\pm x}p_z$	2	0
−9.33	$b_1 + b_2[e_g(\pi^*)]$	$(84)^0$	$\pm 0.38N_{\pm y}p_z$	3	0
−10.91	$b_1[\pi_{O-} - d_{\pi-}]$	$(83)^0$	$0.47d_{xz} - 0.42d_{yz} \mp 0.40(O' + O'')p_x \pm 0.38(O' + O'')p_y$[f]	37	55
−10.97	$a_1[a_{2u}(\pi_N)]$	$(82)^2$	$0.34N_{\pm x}p_z + 0.40N_{\pm y}p_z + 0.23N_\epsilon p_z$	2	5
−11.16	$b_2[d_{\pi+} - \pi_{O+}]$	$(81)^2$	$0.46d_{xz} + 0.48d_{yz} \mp 0.24(O' + O'')p_x \mp 0.27(O' + O'')p_y \pm 0.23(O' + O'')p_z$[f]	44	37
−11.43	$a_2[a_{1u}(\pi_C)]$	$(80)^2$	π (pyrrole carbon) $\sim (0.23, 0.33)Cp_z$	3	0
−11.47	$a_2[b_{2g}(d_{xy})]$	$(79)^2$	$0.90d_{xy} \mp 0.11N_{\pm x}p_y \mp 0.12N_{\pm y}p_x$	78	0
−11.66	$b_1[\pi_{O+} + d_{\pi+}]$	$(78)^2$	$0.37d_{xz} + 0.27d_{yz} \pm 0.23(O' + O'')p_x \pm 0.15(O' + O'')p_y \mp 0.22(O' + O'')p_z$[f]	21	42
−11.68	$b_2[d_{\pi-} + \pi_{O-}]$	$(77)^2$	$0.42d_{yz} - 0.30d_{xz} \mp 0.18(O' + O'')p_x \pm 0.24(O' + O'')p_y$[f]	26	31

[a] Structure II, Figure 2. [b] Energy given in electron volts. [c] Irreducible representation labels from C_{2v} and D_{4h}, where appropriate, although actual symmetry of model is C_s. [d] Coordinate axes defined with Fe in the plane, N (pyrrole nitrogens) along x and y axes, N_ϵ (imidazole nitrogen) along $-z$ axis, and O′ (oxygen atom nearer to iron) along z axis with projection of O″ (oxygen atom further from iron) bisecting the N_y-Fe-N_x angle. d orbitals refer only to Fe. [e] Calculated from a Mulliken population analysis. [f] Coefficients on O″ somewhat greater.

Table III. Eigenvalues and Eigenvectors Calculated for Model Oxyheme[a]

Energy[b]	Symmetry[c]	$(MO)^{occ}$	Principal atomic orbital coefficients[d]	%Fe[e]	%O[e]
−7.79	$a_1[b_{1g}(d_{x^2-y^2})]$	$(87)^0$	$0.79d_{x^2-y^2} \pm 0.38N_{\pm x}p_x \mp 0.38N_{\pm y}p_y$	48	0
−9.01	$b_1 + b_2[e_g(\pi^*)]$	$(86)^0$	$\pm 0.35N_{\pm x}p_z$	2	0
−9.11	$a_1a_{1g}(d_{z^2})]$	$(85)^0$	$0.83d_{z^2} - 0.48N_\epsilon p_z \mp 0.23N_{\pm x}p_x \mp 0.21N_{\pm y}p_y$	58	4
−9.31	$b_1 + b_2[e_g(\pi^*)]$	$(84)^0$	$\pm 0.38N_{\pm x}p_z$	3	0
−10.53	$b_2[\pi_{O+} - d_{\pi+}]$	$(83)^0$	$0.42d_{xz} + 0.40d_{yz} + 0.63(O' - O'')p_z$	15	64
−10.99	$a_1[a_{2u}(\pi_N)]$	$(82)^2$	$0.35N_{\pm x}p_z + 0.41N_{\pm y}p_z + 0.12N_\epsilon p_z$	3	2
−11.18	$b_1[\pi_{O-}]$	$(81)^2$	$0.53(O' - O'')p_x - 0.53(O' - O'')p_y$	0	94
−11.40	$b_2[d_{\pi-}]$	$(80)^2$	$0.59d_{xz} - 0.59d_{yz}$	68	0
−11.42	$a_2[a_{1u}(\pi_C)]$	$(79)^2$	π (pyrrole carbon) $\sim (0.22, 0.31)Cp_z - 0.40d_{xy}$	16	1
−11.46	$a_2[b_{2g}(d_{xy})]$	$(78)^2$	$0.82d_{xy} \mp 0.10N_{\pm x}p_y \mp 0.10N_{\pm y}p_x$	65	0
−11.64	$b_1[d_{\pi+} + \pi_{O+}]$	$(77)^2$	$0.39d_{xz} + 0.39d_{yz} - 0.31(O' - O'')p_z$	30	16

[a] Structure VI, Figure 2. [b] Energy given in electron volts. [c] Irreducible representation labels from C_{2v} and D_{4h}, where appropriate, although actual symmetry of model is C_s. [d] Coordinate axes defined with Fe in the plane, N (pyrrole nitrogens) along x and y axes, N_ϵ (imidazole nitrogen) along $-z$ axis, and projection of O′ and O″ bisecting the N_y-Fe-N_x angle. d orbitals refer only to Fe. [e] Calculated from a Mulliken population analysis.

Table IV. Symmetry Combinations of Iron and Oxygen Atomic Orbitals in the Molecular Orbitals of Oxyheme with Singly or Doubly Coordinated Dioxygen Ligand Geometry

	Atomic orbital mixing[a]	
Orbital label	Singly coordinated	Doubly coordinated
$d_{\pi+}$	$d_{xz} + d_{yz}$	$d_{xz} + d_{yz}$
$d_{\pi-}$	$d_{xz} - d_{yz}$	$d_{xz} - d_{yz}$
π_{O+}	$p_x + p_y - p_z$	p_z
π_{O-}	$p_x - p_y$	$p_x - p_y$

[a] Symmetry combinations are shown for one iron (d orbitals) or one oxygen (p orbitals) center. For the iron-oxygen interaction shown in Figure 3, the two oxygen centers combine in $\pi_O + \pi_O$ fashion. In lower energy oxygen based molecular orbitals, the two oxygen centers combine in $\pi_O - \pi_O$ fashion.

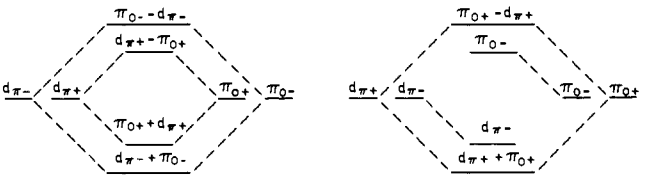

Figure 3. Correlation diagram of iron-dioxygen interaction for end-on singly coordinated conformers and doubly coordinated conformers.

(MO 81) and the lower energy partner π_{O+} character (MO 78). In the doubly coordinated dioxygen ligand geometry, only the $d_{\pi+}$ and π_{O+} orbitals interact significantly. There is much less mixing of the $d_{\pi-}$ and π_{O-} orbitals in this conformation than in the singly coordinated, end-on dioxygen ligand geometry.

Rotation of dioxygen about the Fe-O axis for all geometries or of imidazole about the Fe-N_ϵ axis for the crystal structure (II) leaves the percent of iron and oxygen character in the four orbitals unchanged. However, the relative contributions of the d_{xz} and d_{yz} orbitals to the $d_{\pi+}$ and $d_{\pi-}$ combinations in all four orbitals depend upon the orientation of the dioxygen ligand and in the two lower energy orbitals upon the orientation of the imidazole ligand.

Delocalization of the iron orbitals upon covalent binding to the ligands leads to a net iron atom configuration in the iron(II)-dioxygen complex which differs considerably from a formal low-spin iron(II) configuration. The orbital occupancies calculated by both the iterative extended Hückel and ab initio methods obtained from a Mulliken population analysis of filled molecular orbitals for structures II and VI are given in Table V. Table VI summarizes the extent of forward and back donation between the iron atom and each type of ligand for structure II. Energy levels for the highest filled and lowest empty molecular orbitals of four representative geometries (II, IX, XIV, and XVII) are given in Figure 4. Rotation about the Fe-O axis (II and IX) in a singly coordinated, end-on dioxygen ligand conformation shows little effect on the calculated eigenvalues. The energy of the empty mixed $\pi_O - d_\pi$ orbital is substantially higher in the doubly coordinated dioxygen ligand

Table V. Calculated[a] Occupancies of Iron Atomic Orbitals in Model Oxyheme

Configuration	Atomic orbital								
	4s	$3d_{xy}$	$3d_{xz}$	$3d_{yz}$	$3d_{z^2}$	$3d_{x^2-y^2}$	$4p_x$	$4p_y$	$4p_z$
Low-spin iron(II)	0	2	2	2	0	0	0	0	0
Iterative extended Hückel									
Structure II	0.28	1.99	1.55	1.60	0.87	1.02	0.13	0.14	0.16
Structure VI	0.24	1.99	1.61	1.60	0.90	1.05	0.12	0.13	0.07
Ab initio[b]									
Resembling structure II	0.15	1.91	1.93	1.93	0.22	0.33	0.11	0.11	0.07
Resembling structure VI	0.17	1.91	1.80	1.80	0.31	0.38	0.13	0.13	0.09

[a] Obtained from a Mulliken population analysis. [b] Valence electron contribution estimated by subtracting the contribution of fully occupied core orbitals from the reported total orbital populations (ref 27).

Table VI. Extent of Iron-Ligand Electron Delocalization[a] in Model Oxyheme

	4s	$3d_{xy}$	$3d_{xz}$	$3d_{yz}$	$13d_{z^2}$	$3d_{x^2-y^2}$	$4p_x$	$4p_y$	$4p_z$
				Forward Donation					
$O_2 \rightarrow Fe$	0.06	0.00	0.46	0.48	0.16	0.00	0.01	0.01	0.04
$N_{imid} \rightarrow Fe$	0.10	0.00	0.03	0.06	0.21	0.00	0.07	0.07	0.07
$N_{pyr} \rightarrow Fe$	0.12	0.43	0.61	0.56	0.50	1.02	0.05	0.06	0.05
Total	0.28	0.43	1.10	1.10	0.87	1.02	0.13	0.14	0.16
				Back Donation					
$Fe \rightarrow O_2$		0.00	0.85	0.61					
$Fe \rightarrow N_{imid}$		0.00	0.11	0.01					
$Fe \rightarrow N_{pyr}$		0.44	0.59	0.88					
Total		0.44	1.55	1.50					

[a] Calculated from a Mulliken population analysis.

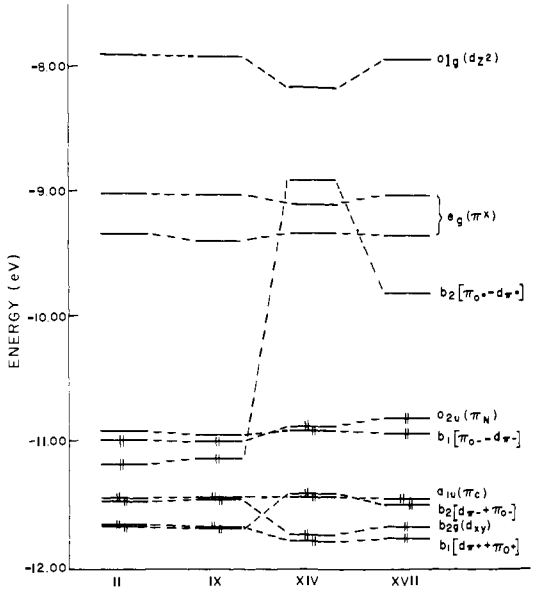

Figure 4. Energy levels calculated for stuctures II, IX, XIV, and XVII.

geometry (XIV), but decreases as the dioxygen ligand is tilted such that the oxygen axis is no longer parallel to the porphyrin plane (XVII).

Promotion energies from selected filled molecular orbitals to the unfilled mixed $\pi_O - d_\pi$ orbital for each dioxygen conformation are given in Table VII. Also included are total energies calculated for each geometry as the sum of the energies of the filled molecular orbitals for the totally paired configuration.

Net atomic charges and iron-ligand and oxygen-oxygen bond overlap densities were obtained by a Mulliken population analysis for each geometry in a totally paired configuration. All atomic charges and all overlap densities except the Fe-O density were insensitive to dioxygen geometry variation. Table VIII gives the average value of the net atomic charge on iron and each ligand atom, of the net group charge on dioxygen, imidazole, and the porphine ring, and of the iron-nitrogen and oxygen-oxygen bond overlap densities. The range for all the geometries is indicated in parentheses. The variation in Fe-O overlap density for three types of dioxygen structures is also shown in Table VIII.

Table IX lists the quadrupole splittings and anisotropy calculated for each dioxygen conformation in a number of different electronic configurations as defined in Table I. Rotation of the imidazole ring in structure II had no effect on the calculated values.

Discussion

The iterative extended Hückel method neglects explicit calculation of two-centered electron repulsion terms. However, the method can be used as a qualitative measure of energy variations as a function of relatively small changes in reasonable geometries and hence might aid in determining the conformation of the oxygen ligand in the heme pocket. Assuming a totally paired iron(II)-dioxygen configuration, all of the total energies calculated for an end-on, singly coordinated dioxygen geometry with a Fe-O-O bond angle greater than 100° (I, II, III, VIII, IX, X, XVIII, XIX, XX, XXI, XXII) are lower than those calculated for a triangular, doubly coordinated dioxygen geometry (VI, VII, XIII, XIV, XV, XVI, XVII). The average energy difference between the two sets of conformations is 2.7 eV. The four end-on conformations with a nearly perpendicular Fe-O-O bond (IV, V, XI, XII) closely resemble doubly coordinated dioxygen geometries and have energies comparable to the latter group. The ab initio calculations of Dedieu et al.[26,27] showed a bent, end-on conformation (resembling structure II) to be 2.39 eV lower in energy than a doubly coordinated dioxygen geometry (resembling structure VI).

Table VII. Total Energies and Promotion Energies (in eV) Calculated for each Dioxygen Ligand Geometry

Structure	Total energy of paired configuration A	Energy required[a] to form configuration B	C	D	E	F
I	−2912.8	0.04	0.12	0.58	0.78	0.78
II	−2912.9	0.25	0.05	0.56	0.75	0.77
III	−2913.4	0.44	0.06	0.54	0.60	0.80
IV	−2911.9	0.36	0.09	0.59	0.51	0.81
V	−2910.2[b]	0.02	0.34	0.67	0.78	0.93
VI	−2910.6[b]	0.59	0.44	0.89	1.11	0.86
VII	−2911.2[b]	1.73	1.49	2.53	2.78	2.35
VIII	−2913.9[b]	0.03	0.10	0.57	0.77	0.76
IX	−2913.6	0.21	0.04	0.54	0.74	0.74
X	−2913.7	0.28	0.03	0.50	0.51	0.69
XI	−2908.7	0.04	0.38	0.44	0.80	0.55
XII	−2910.0[b]	0.43	0.73	0.82	1.15	0.92
XIII	−2910.5[b]	0.64	0.45	0.92	1.10	0.86
XIV	−2911.1[b]	1.97	2.00	2.83	2.98	2.51
XV	−2910.8[b]	1.54	1.64	2.42	2.51	2.16
XVI	−2910.8[b]	1.26	1.38	2.14	2.23	1.92
XVII	−2910.9[b]	0.98	1.12	1.85	1.95	1.67
XVIII	−2914.3	0.46	0.02	0.64	0.84	0.69
XIX	−2914.2	0.48	0.07	0.68	0.65	1.61
XX	−2913.8	0.23	0.05	0.55	0.74	0.76
XXI	−2912.4[b]	0.01	0.13	0.61	0.81	0.78
XXII	−2910.5[b]	0.22	0.03	0.54	0.75	0.72

[a] Calculated from the energy splittings of the orbitals of configuration A with no added correction terms. [b] Configuration A defined with the $[d_{\pi-} - \pi_{O-}]$ orbital doubly occupied and the $[\pi_{O+} - d_{\pi+}]$ orbital unoccupied.

Table VIII. Average Net Atomic Charges, Net Group Charges, and Bond Overlap Densities of Model Oxyheme[a]

Net Atomic Charges	
Fe	0.27 (0.23-0.29)
N_{pyr}	−0.18 (0.11-0.19)
N_ϵ	−0.13 (0.11-0.15)
O′	−0.25 (0.21-0.30)
Net Group Charges	
Dioxygen	−0.56 (0.51-0.61)
Imidazole	0.39 (0.35-0.47)
Porphine	−0.10 (0.00-0.16)
Bond Overlap Densities	
$Fe-N_{pyr}$	0.35 (0.22-0.38)
$Fe-N_\epsilon$	0.30 (0.28-0.32)
O′-O″	0.74 (0.69-0.77)
Fe-O′ (i) End on; $\theta \geq 101°$ [b]	0.39 (0.32-0.41)
(ii) End on; $\theta = 90, 95°$ [c]	0.21 (0.20-0.22)
(iii) Doubly coordinated[d]	0.13 (0.08-0.18)
Fe-O″ (i) End on; $\theta \geq 101°$ [b]	Antibonding
(ii) End on; $\theta = 90, 95°$ [c]	Antibonding
(iii) Doubly coordinated[d]	0.08 (0.04-0.13)

[a] Calculated from a Mulliken population analysis. The range for all geometries is indicated in parentheses. [b] Structures I-IV, VIII-X, and XVIII-XXII. [c] Structures V, XI, and XII. [d] Structures VI, VII, and XIII-XVII.

Thus both extended Hückel and ab initio results favor a bent, end-on dioxygen ligand geometry.

Among these geometries, the iterative extended Hückel results predict the ground state conformation of oxyheme to be structure XVIII. The dioxygen ligand has a tilt nearly comparable to that found in the crystal structure (II) except that the Fe-O bond is not along an axis perpendicular to the heme plane. Instead, the oxygen molecule is displaced such that the iron atom nearly bisects the projection of the O-O bond onto the heme plane. A 20° increase in the tilt of the dioxygen ligand (XIX) has little effect on the energy. Both of these conformers were found to be about 0.5 eV lower in energy than those in which the Fe-O axis is perpendicular to the heme plane as found in the crystal structure. No ab initio calculations are available with which to compare the relative stability of an off-axis displacement of the dioxygen ligand. Due to residual errors and uncertainties in the x-ray structure, the possibility of an off-axis position of the Fe-O bond cannot be neglected.

Besides the off-axis displacement of the dioxygen ligand, two other possible degrees of freedom of the oxygen molecule in an end-on, singly coordinated conformation were considered: variation of the Fe-O-O bond angle (θ) and rotation about the Fe-O axis (dihedral angle $\tau_{N_{pyr}\text{-Fe-O-O}}$). Small energy variations are observed for $\theta = 110$–$160°$, whereas the energy rises sharply outside of this range. For $\tau = 45°$ (structures I-V, XXI), the energy varies within the range by 0.6 eV with a minimum at $\theta = 110°$; for $\tau = 0°$ (structures VIII-XII, XXI), by 0.3 eV with a minimum at $\theta = 160°$. The fact that the bond angle which gives the minimum energy conformation is dependent upon the dihedral angle might indicate a coupling of the vibrational and rotational modes of freedom.

While a relatively small barrier to rotation is observed, the extended Hückel results cannot be used to quantitatively estimate the rotational barrier around the Fe-O axis. Since the method neglects explicit calculation of electron repulsion terms, destabilization of the conformers with $\tau = 0°$ is underestimated. Ab initio calculations indicate a rotational barrier of only 0.24 eV (assuming θ to be constant at 135° and no second axial ligand) with $\tau = 45°$ favored over $\tau = 0°$. Relaxation effects will reduce even further the calculated energy barrier.

The composite description of the dioxygen ligand which emerges from the results of the extended Hückel and ab initio calculations favors a bent, end-on structure with a possible off-axis displacement of dioxygen and a large amplitude bond vibration coupled to a low-energy rotation. Such behavior is consistent with the detection of several different conformers in the x-ray structure[3] and indications of a large thermal disorder in the position of the oxygen molecule.[31]

The electronic ground-state configuration or total spin state cannot be predicted by total energies calculated from the iterative extended Hückel method. The recent ab initio calcu-

Table IX. Variation in Calculated Quadrupole Splittings[a] with Dioxygen Ligand Geometry and Electronic Configuration for Model Oxyheme

	Configuration[b]					
Structure	A	B	C	D	E	F
I	−2.67 (0.41)	1.72 (0.20)	1.56 (0.97)	1.41 (0.57)	1.76 (0.66)	−2.29 (0.52)
II	−2.67 (0.37)	1.88 (0.10)	−1.54 (0.67)	1.51 (0.67)	1.60 (0.57)	−2.27 (0.44)
III	−2.55 (0.37)	1.93 (0.16)	−1.48 (0.62)	−1.21 (0.47)	−1.09 (0.54)	−1.79 (0.53)
IV	−2.43 (0.39)	1.47 (0.45)	−1.43 (0.62)	1.08 (0.80)	1.94 (0.13)	−1.72 (0.56)
V	−1.88 (0.80)	1.25 (0.38)	−1.12 (0.80)	1.71 (0.32)	1.95 (0.35)	1.51 (0.87)
VI	−2.20 (0.48)	−1.27 (0.88)	−1.20 (0.90)	1.16 (0.58)	−2.10 (0.50)	2.36 (0.89)
VII	−2.34 (0.54)	1.17 (0.88)	1.17 (0.94)	1.38 (0.89)	−1.49 (0.90)	−2.51 (0.95)
VIII	−2.77 (0.35)	1.76 (0.27)	−1.62 (0.94)	1.49 (0.40)	−2.31 (0.49)	1.87 (0.99)
IX	−2.74 (0.33)	1.89 (0.06)	−1.60 (0.58)	1.56 (0.51)	1.63 (0.77)	−2.37 (0.38)
X	−2.51 (0.35)	1.54 (0.45)	−1.54 (0.58)	1.06 (0.66)	1.87 (0.26)	−2.32 (0.38)
XI	1.20 (0.98)	−1.67 (0.89)	−2.31 (0.25)	−2.13 (0.32)	1.17 (0.69)	−0.64 (0.71)
XII	−1.20 (0.91)	−1.64 (0.92)	−2.03 (0.28)	−2.17 (0.29)	1.10 (0.50)	−1.03 (0.55)
XIII	−2.20 (0.48)	−1.03 (0.58)	−1.24 (0.86)	1.08 (0.65)	−2.16 (0.49)	2.33 (0.89)
XIV	−2.39 (0.42)	−1.51 (0.17)	−1.84 (0.55)	1.32 (0.25)	−2.25 (0.44)	2.43 (0.39)
XV	−2.26 (0.44)	1.32 (0.46)	−1.38 (0.71)	1.41 (0.47)	−1.80 (0.55)	1.79 (0.63)
XVI	−2.27 (0.43)	1.39 (0.18)	−1.32 (0.83)	1.57 (0.60)	−1.72 (0.65)	1.58 (0.76)
XVII	−2.29 (0.44)	1.45 (0.12)	−1.34 (0.83)	1.64 (0.53)	−1.87 (0.56)	1.46 (0.73)
XVIII	−2.96 (0.38)	1.87 (0.21)	−1.81 (0.87)	1.59 (0.60)	−2.54 (0.45)	1.87 (0.75)
XIX	−2.96 (0.36)	1.93 (0.28)	−1.79 (0.88)	1.51 (0.47)	1.62 (0.65)	−2.45 (0.40)
XX	−2.71 (0.34)	1.89 (0.08)	−1.57 (0.62)	1.54 (0.60)	1.72 (0.92)	−2.25 (0.44)
XXI	−2.63 (0.45)	1.82 (0.03)	−1.53 (0.77)	1.35 (0.56)	−2.32 (0.54)	1.76 (0.48)
XXII	−2.73 (0.36)	1.90 (0.13)	−1.56 (0.67)	1.52 (0.55)	−2.29 (0.44)	1.63 (0.55)

[a] ΔE_Q in millimeters per second calculated from $\Delta E_Q = 8Qq[1 + \eta^2/3]^{1/2}$ with the principal axis values of the field gradient ordered $|V_{ii}| > |V_{jj}| > |V_{kk}|$ such that $q \equiv$ largest magnitude V_{ii} and $\eta \equiv (V_{kk} - V_{jj})/V_{ii}$ $(0 \leq \eta \leq 1)$. Sign of ΔE_Q is sign of largest magnitude V_{ii}. Anisotropy (η) in parentheses. [b] Electronic configurations defined in Table I.

lations[27] have attempted to resolve the uncertainty. With a bent, end-on dioxygen geometry resembling structure II, three electronic configurations were considered: totally paired, $(d_{xy})^1(\pi_{O-} - d_{\pi-})^1$, and $(d_{\pi-} + \pi_{O-})^1(\pi_{O-} - d_{\pi-})^1$. Although a triplet state corresponding to the latter configuration was found to have lowest energy, the differences were small enough that assignment of a ground state was ambiguous. A singlet state arising from a configuration with two unpaired electrons (an antiferromagnetic ground state) was greater yet in energy. However, only two such configurations were considered. Thus, energy calculations to date have not been able to determine the ground-state configuration of oxyheme complexes. It therefore becomes necessary to turn to calculation of electromagnetic properties for further insight. Specifically, electronic and Mössbauer resonance spectra have been cited as the main support for a formal electron transfer, iron(III)-superoxide configuration. Thus it is of central interest to compare observed behavior with properties calculated as a function of electronic configuration and dioxygen ligand geometry to further determine the ground-state characteristics of the oxyheme complex.

Electronic transition energies are two electron properties which cannot be accurately calculated by semiempirical methods. However, calculated orbital promotion energies together with estimated exchange energies from extended Hückel methods have been used successfully in the past for the general assignment of electronic transitions in heme complexes. The orbital promotion energies from various filled orbitals to the empty $(\pi_O - d_\pi)^*$ orbital as shown in Table VII together with the more complete set of eigenvalues and eigenvectors for each geometry considered are being used for possible assignment of the three transitions associated with the dioxygen ligand in single crystal polarized absorption spectra of oxyhemoglobin and oxymyoglobin. As seen in Table VII, orbital promotion energies to the $(\pi_O + d_\pi)^*$ orbital are very sensitive to dioxygen ligand geometry. To date, no one geometry has as yet given a unique fit to the spectra. However, preliminary results do seem to rule out a biradical ground state with a single electron in the $(\pi_O + d_\pi)^*$ orbital.[12] More detailed results will be reported elsewhere.

While two-electron properties are not reliably calculated by the iterative extended Hückel method, one-electron properties such as the electric field gradient tensor at the iron nucleus can be reliably estimated from the calculated eigenvectors. We have thus calculated the field gradient at the iron nucleus observed as quadrupole splitting in Mössbauer resonance for all geometries considered in a number of possible electronic configurations.

As shown in Table IX, a large negative value for the quadrupole splitting is obtained from a low-spin iron(II)-dioxygen configuration (A), in agreement with the observed low-temperature value of −2.24 mm/s for the protein and −2.10 mm/s for the model compounds with $\eta \leq 0.5$. In this configuration, the only conformations which do not yield a large negative value (V, XI, and XII) have very distorted Fe-O-O bond angles with a bent, end-on dioxygen ligand geometry. None of the five other electron transfer configurations give consistent agreement with experiment. Thus, while energy criteria cannot resolve the electronic ground-state configuration, observed one-electron properties can systematically be accounted for only by an iron(II)-dioxygen ground-state configuration.

The quadrupole splittings calculated for the singly coordinated, end-on dioxygen geometries decrease slightly with decreasing Fe-O-O bond angle (I-V and VIII-XII) and increase slightly upon rotation about the Fe-O bond (I, VIII and II, XX, IX). However, no substantial variation with dioxygen geometry is observed for a normal bent conformation. The values calculated for the doubly coordinated dioxygen ligand are all lower in magnitude, in better agreement with experiment. Thus while energy criteria favor a bent, end-on structure over a doubly coordinated dioxygen ligand geometry, the calculated field gradients cannot further resolve the uncertainties in the ground-state conformation of the dioxygen ligand.

Table X. Comparison between Calculated and Observed Temperature Dependence of the Quadrupole Splitting of Oxyheme

	ΔE_Q (low T)[a]	ΔE_Q (high T)[a]	High T/low T
		Experimental	
Model	−2.10	1.34	0.64
Protein	−2.24	1.89	0.84
		Calculated	
Model	−2.67	1.80 (V_{zz})[b]	0.67
Protein	−2.67	−2.40 (V_{xx}, V_{yy})[c]	0.90

[a] ΔE_Q in millimeters per second. [b] Largest component of the field gradient is perpendicular to the porphine plane. [c] Largest component of the field gradient is in the porphine plane.

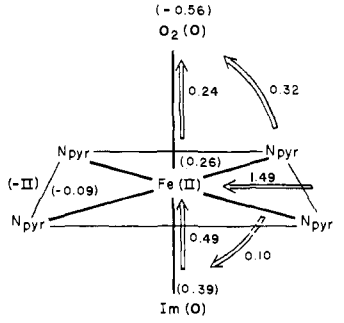

Figure 5. Formal valences and actual group charges calculated from a Mulliken population analysis showing extent of forward donation and backbonding in model oxyheme.

Both oxyhemoglobin and the model oxyheme compounds show a reduction in the observed quadrupole splitting with increasing temperature. The high-temperature value for the protein is 1.89 mm/s; for the model compound, 1.34 mm/s. The observed temperature dependence of the quadrupole splitting may be accounted for by rotation around the Fe–O axis in a singly coordinated, end-on dioxygen ligand geometry.

Low-energy rotation in the model compound appears possible with contributions to the field gradient from all values of τ at higher temperatures. If this rotation is approximated by averaging the contributions to the nine components of the field gradient from the two conformers found in the crystal structure II and XXII, a reduction of the quadrupole splitting to +1.80 mm/s with $\eta = 0.02$ is obtained. On the other hand, in oxyhemoglobin the heme pocket might not accommodate such large rotational variation in τ. (A recent Fourier difference spectra of carboxyhemoglobin has led to predictions of a bent, end-on Fe–O–O geometry for the oxy complex with $\tau \simeq 0$–45°.)[32] Assuming limited rotational freedom of τ = 0–45°, the contributions to the nine components of the field gradient from conformers II, IX, and XX are averaged, yielding a reduction of the quadrupole splitting to −2.40 mm/s with $\eta = 0.57$.

Assuming conformer II to be the low energy form of both oxyhemoglobin and model oxyheme, the ratios of the calculated high-temperature values to the low-temperature value of the quadrupole splitting as shown in Table X compare favorably to those observed for the protein and the model compound. Free rotation about the Fe–O axis in the model compounds leads to a greater observed temperature dependence than possible hindered rotation in the heme pocket of the protein. If the postulated origin of the temperature dependence of the quadrupole splitting is correct, in the model compound the high-temperature value would have a positive sign with the principal axis value perpendicular to the heme plane. In the protein the high-temperature value would remain negative with the principal axis value in the plane of the porphine ring. Averaging of bond angle variations at a given dihedral angle showed no cancellation of the field gradient components, no reduction of the principal axis values, and therefore no reduction of the calculated quadrupole splitting. Possible low-energy vibrations of the Fe–O–O bond would not affect the observed temperature dependence.

Thus a totally paired iron(II)–dioxygen configuration can account for the magnitude, sign, and temperature dependence of the observed quadrupole splitting. Although a formally low-spin iron(II) configuration $[(d_{xy})^2(d_{xz})^2(d_{yz})^2(d_{z^2})^0(d_{x^2-y^2})^0]$ would yield a spherically symmetric charge distribution around the iron nucleus and result in a vanishingly small quadrupole splitting, due to covalency upon binding with the ligands the actual distribution around the iron in the ferrous oxyheme complex as shown in Table V differs significantly from spherical symmetry. As indicated in Table VI, the occupation of the d_{xy} orbital remains nearly equal to two with an equal extent of forward donation into the d_{xy} orbital and back donation from the d_{xy} orbital upon bonding between iron and the pyrrole nitrogens. The d_{z^2} and $d_{x^2-y^2}$ orbitals, formally unoccupied, are populated by forward donation upon σ and π bonding to the axial ligands and the pyrrole nitrogens in lower lying ligand-based molecular orbitals. Therefore, despite its formal divalent state, the iron atom has a calculated charge that is only slightly positive as shown in Figure 5.

A larger degree of backbonding from iron to dioxygen than forward donation into the d_{xz} and d_{yz} orbitals upon π bonding to the dioxygen ligand results in a net negative charge on dioxygen. The total net charge of −0.5 e on the dioxygen ligand is due to additional donation of electrons from the pyrrole ring. The partial negative charge on dioxygen predicted by the iterative extended Hückel method is consistent with the displacement of dioxygen by excess anionic ligands and is a manifestation that some superoxide anionic character is possible even in a formal Fe(II)–O_2 configuration.

The ab initio calculation gives a nearly neutral dioxygen ligand and a net positive charge of 1.23 e on the iron. The orbital densities calculated from ab initio results listed in Table V show less delocalization of the iron orbitals upon backbonding to or forward donation from the ligands. However, it is inappropriate to compare net charges calculated from population analyses of different basis set functions. Calculated electronic density within given atomic radii would be basis set independent and would allow such comparisons.

As shown in Table VIII, the single iron–oxygen bond overlap density in a bent, end-on structure is larger than the sum of both iron–oxygen overlap densities in a doubly coordinated structure. In the bent, end-on conformations the dioxygen ligand has a small degree of σ bonding with the d_{z^2} orbital of iron and a much larger degree of π bonding with the d_{xz} and d_{yz} orbitals of iron. The extent of π bonding remains unchanged with rotation of either axial ligand, but the relative contributions of the d_{xz} and d_{yz} orbitals to the bonding is affected. In the doubly coordinated structures, the total π bonding interaction is diminished.

It is interesting to note that the O–O bond overlap density is unaffected by dioxygen ligand geometry provided the O–O bond length remains nearly constant. Previous investigations have discriminated between Pauling and Griffith type structures or the basis of a lower infrared stretching frequency for the latter.[6] However, the results suggest that a lower frequency for a doubly coordinated complex may be more a consequence of a longer O–O bond than differences in the bonding interaction itself.

Conclusion

Both ab initio and iterative extended Hückel calculations favor a bent, end-on (Pauling) structure over a doubly coor-

dinated (Griffith) structure for the dioxygen ligand geometry on the basis of total energies. For the bent, end-on structure, low-energy off-axis displacement of the dioxygen ligand and a low barrier to rotation about the Fe-O axis possibly coupled to a large amplitude bending mode of the Fe-O-O bond lead to a conformational flexibility of the dioxygen ligand. Both total and molecular energy values calculated from ab initio and iterative extended Hückel methods fail to resolve the uncertainties in the electronic ground-state configuration. However, only a totally paired iron(II)-dioxygen configuration can consistently account for the large negative electric field gradient at the iron nucleus observed as quadrupole splitting in Mössbauer resonance. In addition, the temperature dependence of the quadrupole splitting may be accounted for by rotation about the iron-oxygen bond. Due to covalency upon binding of iron to the ligands, the calculated electron distribution around the iron differs substantially from a low-spin iron(II) configuration. Finally, a large net negative charge calculated for the dioxygen ligand indicates possible superoxide character even without a charge transfer iron(III)-superoxide configuration.

Acknowledgment. This research was supported by National Science Foundation Grant PCM76-07324. Helpful discussions with Dr. Leonard Hjelmeland, Stanford University, are gratefully acknowledged. We are also grateful to Charles J. Kert, Stanford University, for his assistance in the compilation and analysis of the results.

References and Notes

(1) J. P. Collman, R. R. Gagné, C. A. Reed, W. T. Robinson, and G. A. Rodley, *Proc. Natl. Acad. Sci. U.S.A.*, **71**, 1326 (1974).
(2) G. Lang and W. Marshall, *Proc. Phys. Soc.*, **87**, 3 (1966).
(3) J. P. Collman, R. R. Gagné, C. A. Reed, T. R. Halbert, G. Lang, and W. T. Robinson, *J. Am. Chem. Soc.*, **97**, 1427 (1975).
(4) L. Pauling and C. D. Coryell, *Proc. Natl. Acad. Sci. U.S.A.*, **22**, 210 (1936).
(5) M. W. Makinen and W. A. Eaton, *Ann. N.Y. Acad. Sci.*, **206**, 210 (1973).
(6) C. H. Barlow, J. C. Maxwell, W. C. Wallace, and W. S. Caughey, *Biochem. Biophys. Res. Commun.*, **55**, 91 (1973).
(7) W. C. Wallace, J. C. Maxwell, and W. S. Caughey, *Biochem. Biophys. Res. Commun.*, **57**, 1104 (1974).
(8) J. J. Weiss, *Nature (London)*, **202**, 83 (1964).
(9) J. J. Weiss, *Nature, (London)*, **203**, 183 (1964).
(10) J. B. Wittenberg, B. A. Wittenberg, J. Peisach, and W. E. Blumberg, *Proc. Natl. Acad. Sci. U.S.A.*, **67**, 1846 (1970).
(11) T. G. Spiro, *Biochim. Biophys. Acta*, **416**, 169 (1975).
(12) M. W. Makinen, University of Chicago, Chicago, Illinois, personal communication.
(13) A. K. Churg and M. W. Makinen, *Fed. Proc.*, **35**, 1604 (1976).
(14) L. Pauling, *Nature (London)*, **203**, 182 (1964).
(15) J. S. Griffith, *Proc. R. Soc. Londor, Ser. A*, **235**, 23 (1956).
(16) M. Zerner, M. Gouterman, and H. Kobayashi, *Theor. Chim. Acta*, **6**, 363 (1966).
(17) M. Weissbluth and J. E. Maling, *J. Chem. Phys.*, **47**, 4166 (1967).
(18) S. Aronowitz, M. Gouterman, and J. C. W. Chien, *Theor. Chim. Acta*, submitted for publication.
(19) M. P. Halton, *Theor. Chim. Acta*, **24**, 89 (1972).
(20) M. P. Halton, *Inorg. Chim. Acta*, **8**, 131 (1974).
(21) Y. Seno, J. Otsuka, O. Matsuoka, and N. Fuckikami, *J. Phys. Soc. Jpn.*, **33**, 1645 (1972).
(22) J. Otsuka, O. Matsuoka, N. Fuckikami, and Y. Seno, *J. Phys. Soc. Jpn.*, **35**, 854 (1973).
(23) W. A. Goddard and B. D. Olafson, *Proc. Natl. Acad. Sci. U.S.A.*, **72**, 2335 (1975).
(24) G. Herzberg, *Naturwissenschaften*, **20**, 577 (1932).
(25) H. R. Zeller and W. Känzig, *Helv. Phys. Acta*, **40**, 845 (1967).
(26) A. Dedieu, M.-M. Rohmer, and A. Veillard, *J. Am. Chem. Soc.*, **98**, 3717 (1976).
(27) A. Dedieu, M.-M. Rohmer, and A. Veillard, *Proc. 9th Jerusalem Symp. Quant. Chem. Biochem.*, in press.
(28) G. H. Loew and R. F. Kirchner, *J. Am. Chem. Soc.*, **97**, 7388 (1975).
(29) W. T. Robinson, University of Canterbury, Christchurch, New Zealand, supplied the x-ray coordinates for the model oxyheme compound.
(30) G. H. Loew and D. Y. Lo, *Theor. Chim. Acta*, **33**, 137 (1974).
(31) K. Spartalian, G. Lang, J. P. Collman, R. R. Gagné, and C. A. Reed, *J. Chem. Phys.*, **63**, 5375 (1975).
(32) E. J. Heidner, R. C. Ladner, and M. F. Perutz, *J. Mol. Biol.*, **104**, 707 (1976).

Nybomycin. 9. Synthetic and Biosynthetic Incorporation of ^{15}N as a Means of Assigning the ^{13}C Nuclear Magnetic Resonance Spectrum of Nybomycin[1,2]

Alex M. Nadzan[3] and Kenneth L. Rinehart, Jr.*

Contribution from Roger Adams Laboratory, University of Illinois, Urbana, Illinois 61801. *Received April 6, 1976*

Abstract: The ^{13}C NMR spectrum of the antibiotic nybomycin (**1**) has been assigned unambiguously. Difficult central ring carbon assignments were made by incorporating ^{15}N biosynthetically and employing ^{13}C-^{15}N coupling constants. Other carbon assignments were made from off-resonance proton decoupling, model compound studies, and long range ^{13}C-^{1}H splitting patterns.

Our continuing biosynthetic investigation[2] of the antibiotic nybomycin (**1**) has required assignment of the ^{13}C NMR spectrum of nybomycin *n*-butyrate (**2**) to interpret the results

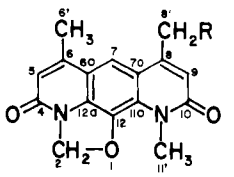

1: R=OH
2: R=$O_2C\overset{1''}{C}H_2\overset{2''}{C}H_2\overset{3''}{C}H_2\overset{4''}{C}H_3$

of ^{13}C precursor labeling experiments. Early studies of the biosynthesis dealt with the incorporation of labeled acetate and methionine into carbons 2, 4, 5, 6, 6′, 8, 8′, 9, 10, 11′, i.e., into the peripheral carbons of the antibiotic.[2b,c] For these studies it was sufficient to identify the peripheral ring carbons (in pairs) and less important to distinguish C-4 from C-10, C-5 from C-9, C-6 from C-8, since they were labeled symmetrically by acetate, or to assign the central ring carbons definitively, since they were unlabeled. However, later biosynthetic studies demonstrating incorporation of glucose and pyruvate into the central ring[2a] required complete, unambiguous assignment of C-6a, C-7, C-7a, C-11a, C-12, and C-12a and a more extensive investigation of the ^{13}C NMR spectrum of nybomycin was undertaken.